Rare Metal Materials and Engineering
Volume 51, Issue 7, July 2022
Available online at www.rmme.ac.cn

Science Press

Cite this article as: Tian Shiwei, He Anrui, Liu Jianhua, et al. Effect of Mo Element on Microstructure and Mechanical Properties of TiAl Alloys[J]. Rare Metal Materials and Engineering, 2022, 51(07): 2336-2343.

ARTICLE

Effect of Mo Element on Microstructure and Mechanical Properties of TiAl Alloys

Tian Shiwei[1], He Anrui[1], Liu Jianhua[1], Zhang Yefei[1], Zhang Yun[1], Yang Yonggang[1,2], Wang Jiayi[3], Jiang Haitao[1]

[1] Institute of Engineering Technology, University of Science and Technology Beijing, Beijing 100083, China; [2] Department of Materials Science and Engineering, KTH Royal Institute of Technology, Stockholm SE-10044, Sweden; [3] College of Engineering, Yantai Nanshan University, Yantai 265713, China

Abstract: Four TiAl alloys with different Mo contents were designed, and the microstructure and mechanical properties of these Mo-TiAl alloys were studied by scanning electron microscope, nanoindentation, and hot compression simulation methods. Results show that with increasing the Mo content, the content of γ phase is gradually decreased, while that of β phase is gradually increased. The Mo element mainly exists in the form of β phase in the TiAl alloy. During the hot isostatic pressing process, the Mo element is diffused from the γ and α_2 phases to the β phase. The nanoindentation hardness of Mo-TiAl alloy reaches the maximum when the Mo content is 1.59at%, and it is negatively correlated with the interlamellar space. As the content of Mo element increases, the flow stress of Mo-TiAl alloys decreases, and the TiAl alloys with 2.11at% and 3.94at% Mo addtion have poor plasticity due to the Al element segregation.

Key words: TiAl alloy; Mo element; microstructure; nanoindentation; segregation

TiAl alloys attract much attention due to their excellent properties, such as low density, high strength, good oxidation resistance, and creep resistance[1-4]. As an intermetallic compound, TiAl alloy has few movable slip systems, thus leading to poor plasticity[5,6]. The amelioration in chemical composition and microstructure to improve the plasticity of TiAl alloy has attracted much attention[7-10]. Concerning the effect of alloying elements on the microstructure and mechanical properties of TiAl alloys, Imayev et al[11] found that when the Al content is greater than 44at%, the lamellar phases are coarse; otherwise, the lamellar grains are fine and have different orientations. Banumathy et al[12] found that the addition of Nb element can refine the lamellar phase size of TiAl alloys and improve the high-temperature deformation ability of TiAl alloy by introducing more β phases. Besides, B and Y elements can also be added into the TiAl alloys. During the solidification process, the B atoms combine with Ti atoms to form the TiB_2 compound, which restricts the growth of the α phase, and increases the heterogeneous nucleation sites of α phase during $\beta \rightarrow \alpha$ phase transformation, resulting in the finer microstructure[13,14]. Y atoms combine with Al atoms to form YAl and YAl_2[15,16], which have a similar refinement effect to TiB_2's. Moreover, the addition of Y element can improve the oxidation resistance of TiAl alloy.

Clemens et al[17] revealed that the β phase stabilization effect of the Mo element is four times better than that of the Nb element. Therefore, the influence of Mo element on the microstructure and mechanical properties of TiAl alloys should be further investigated. In this research, four TiAl alloys containing different contents of Mo element were designed, and the effect of Mo addition on the microstructure of TiAl alloys was studied. In addition, the distribution of Mo element in each phase was analyzed. The effect of Mo element on the nanoindentation hardness and compression deformation behavior of TiAl alloy was also studied.

Received date: July 07, 2021
Foundation item: Shandong Provincial Natural Science Foundation (ZR201911180051); Guangxi Special Funding Program for Innovation-Driven Development (GKAA17202008); National Natural Science Foundation of China (52004029)
Corresponding author: Jiang Haitao, Ph. D., Professor, Institute of Engineering Technology, University of Science and Technology Beijing, Beijing 100083, P. R. China, Tel: 0086-10-62332598-6781, E-mail: jianght@ustb.edu.cn

1 Experiment

Four Mo-TiAl alloys with different Mo contents (TNM1~TNM4) were designed, and their chemical composition is shown in Table 1. The Mo-TiAl alloys were produced by a vacuum suspension melting furnace. The casting size of the ingots was Φ110 mm×170 mm. Then the as-cast Mo-TiAl ingots were heat treated at 900 ℃ for 50 h followed by furnace cooling to room temperature to ensure the chemical homogenization. Then the ingots were treated by hot isostatic pressing (HIP) at 1250 ℃ for 1.5 h and at 1350 ℃ for 2.5 h under the pressure of 175 MPa to improve the densification.

The nanoindentation test was conducted on the Nano-Indenter XP nanoelectron probe. The hot compression test was conducted on the Gleeble-3500 simulator at 1200 ℃ with the strain rates of 0.001, 0.01, 0.1, and 1 s^{-1}. The microstructure observations were conducted on QUANTA 450FEG field emission scanning electron microscope (SEM) and TecnaiG2 F30 field emission transmission electron microscope (TEM). The backscattered electron (BSE) mode was used, and the working voltage was 5.0 V. The constituent phases of TiAl alloys were detected by D8 ADVANCE X-ray diffractometer (XRD) with Cu Kα. The scanning speed was about 3°/min, the scanning step was 0.02°, and the scanning angle ranged from 20° to 90°. The Jade 6.0 software was used for subsequent data processing and analysis.

2 Results and Discussion

2.1 Effect of Mo element on microstructures of Mo-TiAl alloys

Fig.1 shows XRD patterns of the four Mo-TiAl alloys with different Mo contents. It can be seen that the four specimens are composed of γ-TiAl, α_2-Ti_3Al, and β phase. The diffraction peak at 2θ=38.6° represents the γ-(111) phase and has the highest intensity, indicating the largest volume fraction of the γ phase among these phases in the alloys. With increasing the Mo content, the diffraction peak intensity of β/B2-(110) phase (2θ=39.7°) is gradually increased, indicating that the content of β phase in Mo-TiAl alloys is increased significantly.

Fig.2 shows the as-cast microstructures of the four Mo-TiAl alloys. Due to the difference in atomic number, the γ, α_2, and β phases show different contrast colors: the bright white is the β phase, the dark black is the γ phase, and the gray is α_2 phase. The bright white β phase is mainly distributed at the lamellae boundary. The γ phase mainly exists in the form of γ/α_2 lamellae, and some of them are distributed at the phase boundary. As for the α_2 phase, it mainly appears in the form of γ/α_2 lamellae, so it is difficult to solely observe.

Table 1 Chemical composition of Mo-TiAl alloy specimens with different Mo additions (at%)

Specimen	Al	Nb	Mo	B	Y	Ti
TNM1	43.76	4.03	1.02	0.09	0.10	Bal.
TNM2	44.25	3.84	1.59	0.10	0.10	Bal.
TNM3	44.68	4.09	2.11	0.08	0.10	Bal.
TNM4	43.39	3.90	3.94	0.12	0.10	Bal.

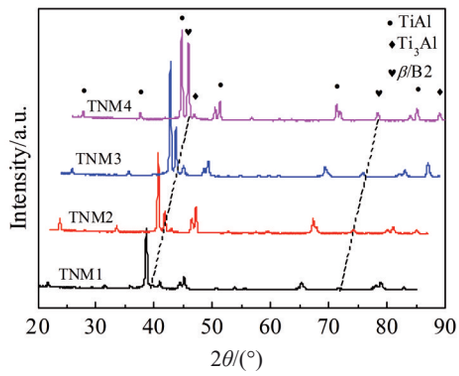

Fig.1 XRD patterns of different as-cast Mo-TiAl alloys

It can be seen from Fig.2a that β and γ phases are scattered around the γ/α_2 lamellae. With increasing the Mo content to 1.59at%, the content of β and γ phases around the lamellae is increased, and the increase in β phase content is particularly obvious (Fig.2b).

As the Mo content further increases, some of the γ/α_2 lamellae in TNM3 and TNM4 alloys are transformed into the cluster structure, as shown in Fig. 2c and 2d, respectively. Fig. 3 shows TEM microstructure and selected area electron diffraction (SAED) pattern of the cluster. It can be seen that the cluster surrounding the γ/α_2 lamellae in Mo-TiAl alloys consists of coexistent $\gamma+\alpha_2+\beta$ phases, which is mainly caused by the chemical imbalance during the smelting process. The existence of the $\gamma + \alpha_2 + \beta$ coexistent phase refines the microstructure to a certain extent. Cha et al[18] found a coexistent phase, which is similar to that in this research, in the Mo-TiAl alloy after heat treatment at eutectoid temperature. The coexistent phases have the following coherent relationship: $\{110\}\beta_0<111>\ \beta_0//(2\bar{1}\bar{1}0)\omega[0001]\omega//(0001)\alpha_2[2\bar{1}\bar{1}0]\alpha_2//\{111\}\gamma<110]\gamma$. Thus, it can be inferred that the coexistent phase is formed by consuming α_2 and γ phases in the γ/α_2 lamellae.

Fig.4 shows the SEM microstructures of the four Mo-TiAl alloys after HIP. TNM1 and TNM2 specimens have relatively uniform microstructure, while the dark band-shaped regions can be observed in TNM3 and TNM4 alloys, indicating the existence of element segregation. Generally, there are three types of element segregation in TiAl alloys: β-type segregation, α-type segregation, and S-type segregation[19-21]. The β-type segregation mainly occurs at the periphery of γ/α_2 lamellae, and it originates from the high-Nb area caused by the transformation from β to α phase. The α-type segregation mainly occurs inside the lamellae. When the content of β phase stabilization elements is high, the $\alpha\rightarrow\alpha_2+\gamma+\beta$ reaction occurs, resulting in the precipitation of β phase particles inside the lamellae. The S-type segregation is formed by the segregation of Al elements in the dendrite during the solidification process, and it is often accompanied with uneven lamellar structure and lamellae coarsening. The dark

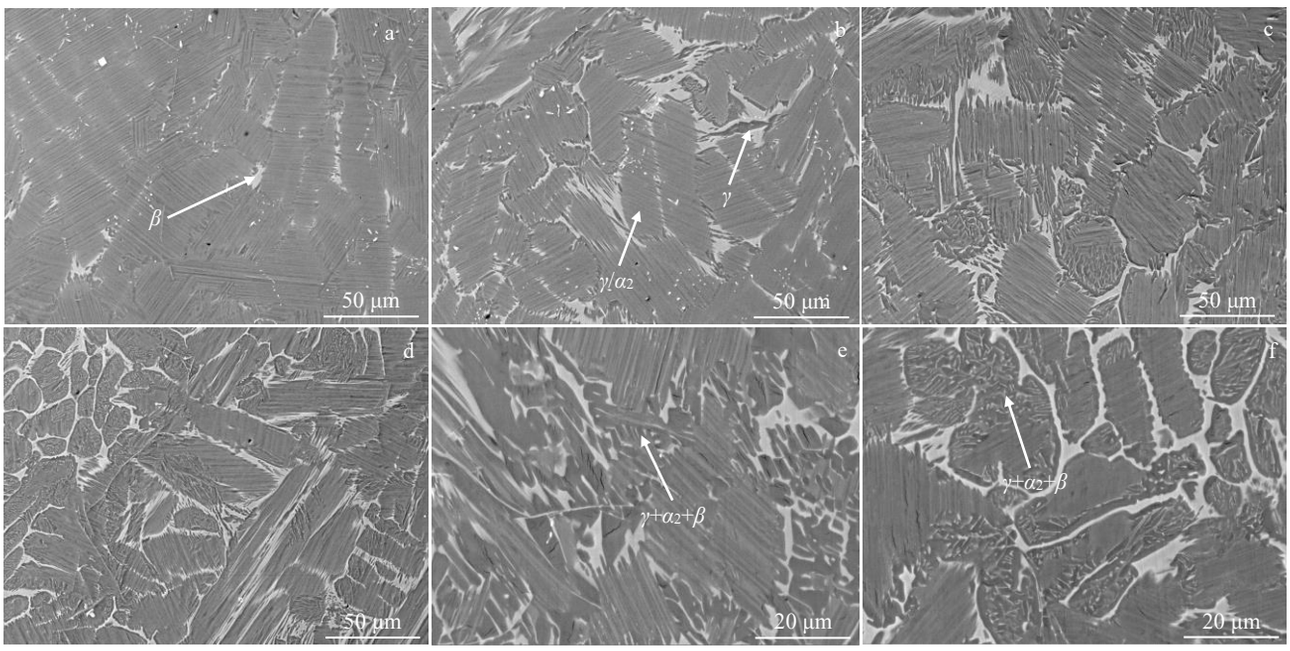

Fig.2 BSE microstructures of different as-cast Mo-TiAl alloys: (a) TNM1, (b) TNM2, (c, e) TNM3, and (d, f) TNM4

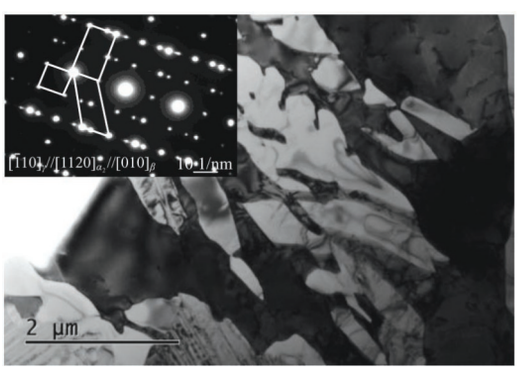

Fig.3 TEM microstructure and SEAD pattern of coexistent $\gamma+\alpha_2+\beta$ phase

areas in Fig. 4c and 4d indicate the area with concentrated Al element, i. e., the S-type segregation occurs in TNM3 and TNM4 specimens. This S-type segregation exists in Mo-TiAl alloys after HIP treatment, and it will adversely affect the mechanical properties of Mo-TiAl alloys.

Fig. 5 shows the magnified microstructures of Mo-TiAl alloys after HIP. It can be seen that the dark areas around the γ/α_2 lamellae in these four Mo-TiAl alloys are enlarged, compared with those in the as-cast Mo-TiAl alloys, indicating that the content of γ phase is slightly increased. The β and γ phases appear as sharp strips around the γ/α_2 lamellae in the as-cast alloys, whereas they are partially spheroidized in the form of block or sphere in the alloys after HIP. It can be seen from Fig. 5c that the volume fraction of the $\gamma+\alpha_2+\beta$ coexistent phase in TNM3 specimen significantly reduces. Fig. 5d shows that the volume fraction of γ/α_2 lamellar phase in TNM4 specimen decreases significantly, and the microstructure is mainly composed of equiaxed γ and β phases. Besides, a large amount of β phase precipitation appears in the γ/α_2 lamellae.

2.2 Enrichment behavior of β-phase stabilization elements in each phase

The γ, α_2, and β phases in the initial TiAl alloys have different chemical composition. After the Mo addition, the chemical composition of these three phases also changes. β phase is easy to detect, since it is distributed at the lamellae boundary. The γ and α_2 phases can only be distinguished in the magnified images, as shown in Fig.6.

The phase composition of Mo-TiAl alloys before and after HIP is shown in Table 2 and Table 3, respectively. It should be mentioned that due to the small content of B and Y elements, the measurement error is considerable. Thus, only the four main elements (Ti, Al, Nb, and Mo) are statistically analyzed.

It can be seen from Table 2 that the content of Ti and Al in the γ phase of the as-cast Mo-TiAl alloys is very close, and the ratio of Ti/Al is within 0.96~1.04. With increasing the Mo content, the ratio of Ti/Al in γ phase is gradually decreased. The ratio of Ti/Al in β phase of as-cast Mo-TiAl alloys is 1.31~1.47. The Nb content in the β phase is 4.02at%~4.35at%, which is higher than that in the γ phase (3.23at%~3.75at%) and in the α_2 phase (3.09at%~3.69at%), indicating that Nb is enriched in the β phase. With increasing the Mo content, the Mo content in the β phase is increased obviously, which is about 3~4 times larger than that in γ phase and α_2 phase. Therefore, it can be concluded that the Mo element mainly exists in the β phase.

In the α_2 phase, the ratio of Ti/Al is 1.11~1.44. Besides, the content of Nb and Mo in the α_2 phase is close to that in the γ phase. It should be noted that with increasing the Mo content, the enrichment of Nb element in the β phase is barely affected.

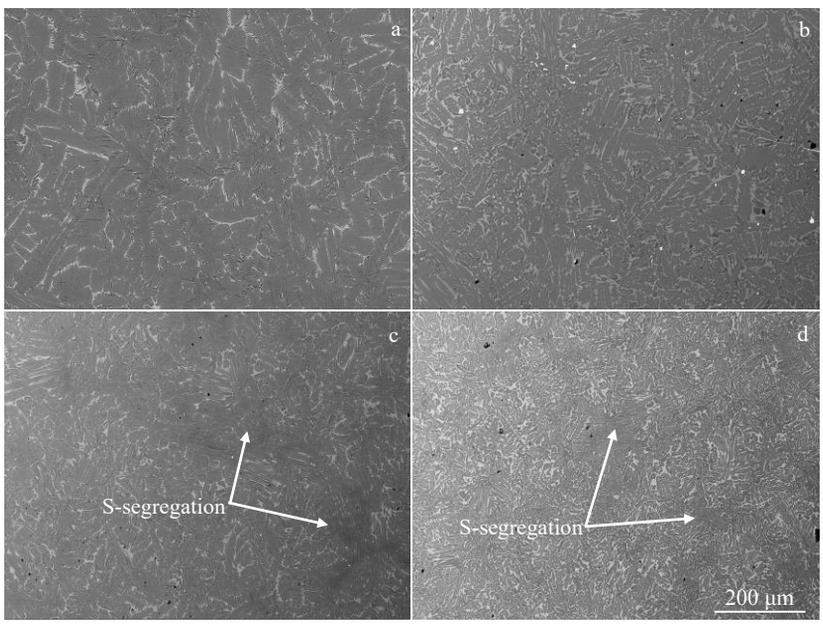

Fig.4 SEM microstructures of different Mo-TiAl alloys after HIP: (a) TNM1, (b) TNM2, (c) TNM3, and (d) TNM4

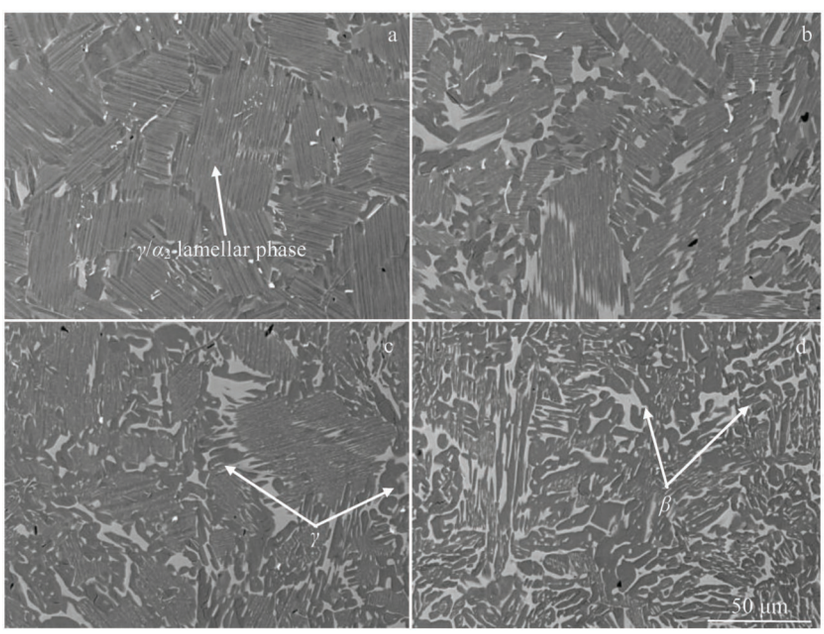

Fig.5 Magnified microstructures of different Mo-TiAl alloys after HIP: (a) TNM1, (b) TNM2, (c) TNM3, and (d) TNM4

According to Table 3, it can be found that after HIP treatment, the Mo element content in the γ and α_2 phase decreases, while that in the β phase further increases. This phenomenon implies that the Mo element is diffused from the γ and α_2 phases to the β phase during HIP process. According to Table 2 and Table 3, with increasing the Mo content, the Ti content in the γ phase shows an overall downward trend, indicating that Mo atoms replace the Ti atoms in the γ phase matrix. Jiang et al[22] used the first-principles theory to calculate the occupancy of 3d, 4d, and 5d transition metal atoms in TiAl alloys, and found that the atoms, such as Zr and Hf, preferentially occupy the positions of Ti atoms. For Nb and Mo atoms, their occupancy status changes with their doping concentration and temperature. Huang et al[23] used the tight-binding energy band method to calculate the bonding strength of TiAl alloys after adding alloying elements, and predicted that most Mo atoms tend to replace Ti atoms, while a few Mo atoms replace Al atoms. Holec et al[24] performed the element doping calculations for binary TiAl alloys and found that the V, Cr, Nb, and Mo elements preferentially replace Ti atoms in γ and α_2 phases, whereas they preferentially replace Al atoms in β phase. The B and C elements are located in the interstitial positions of Ti-rich octahedrons. These calculation results are consistent with the results in this research.

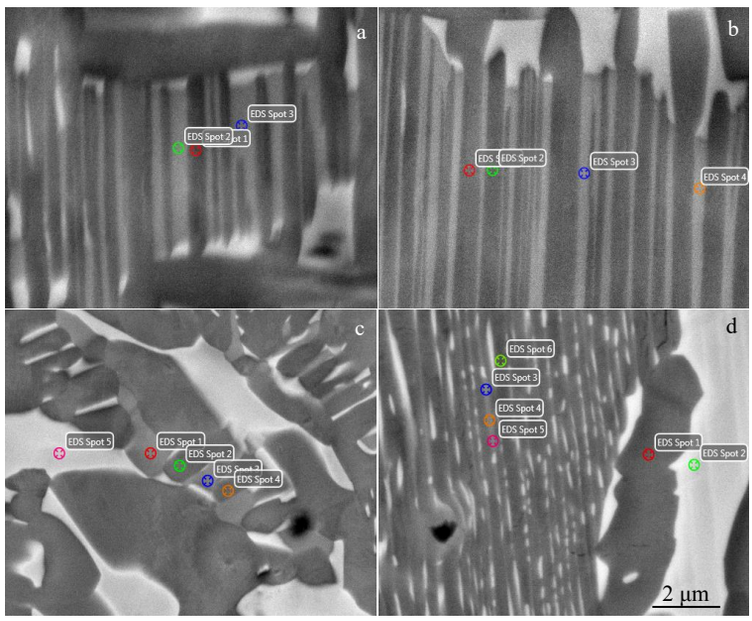

Fig.6 SEM images for phase component analyses of different Mo-TiAl alloys: (a) TNM1, (b) TNM2, (c) TNM3, and (d) TNM4

Table 2 Chemical composition of γ, β, and α_2 phases in different as-cast Mo-TiAl alloy specimens (at%)

Phase	Specimen	Ti	Al	Nb	Mo
γ	TNM1	48.34	46.66	3.75	0.94
	TNM2	48.13	47.71	3.23	1.01
	TNM3	46.81	48.14	3.58	1.25
	TNM4	46.15	47.95	3.49	2.19
β	TNM1	52.87	39.92	4.26	2.61
	TNM2	55.39	37.61	4.02	2.66
	TNM3	52.76	37.46	4.35	5.22
	TNM4	50.41	38.45	4.18	6.77
α_2	TNM1	52.78	42.63	3.55	1.04
	TNM2	54.56	41.06	3.09	0.92
	TNM3	55.93	38.75	3.69	1.63
	TNM4	50.16	44.48	3.38	1.98

Table 3 Chemical composition of γ, β, and α_2 phases in different Mo-TiAl alloy specimens after HIP (at%)

Phase	Specimen	Ti	Al	Nb	Mo
γ	TNM1	47.97	47.47	3.59	0.98
	TNM2	48.06	47.47	3.43	0.75
	TNM3	46.42	48.91	3.12	1.23
	TNM4	44.92	49.15	3.59	1.98
β	TNM1	54.57	37.94	4.39	2.84
	TNM2	55.17	37.08	4.31	3.13
	TNM3	51.93	38.06	4.01	5.67
	TNM4	49.89	38.35	3.72	7.68
α_2	TNM1	52.18	43.64	3.27	0.71
	TNM2	53.52	42.29	3.20	0.90
	TNM3	55.61	39.54	3.16	1.57
	TNM4	49.79	44.93	3.18	1.97

2.3 Nanoindentation hardness

In the nanoindentation test, most of the test points are on the γ/α_2 lamellar phases, and the nanoindentation hardness is closely related to the size of the γ/α_2 interlamellar space. It should be noted that the volume fractions of γ/α_2 lamellae in these four Mo-TiAl alloys are different. In order to accurately describe the relationship between the nanoindentation hardness and the γ/α_2 interlamellar spacing, it is necessary to exclude the difference in hardness caused by the microstructure changes. The average nanoindentation hardness of the TNM1, TNM2, TNM3, and TNM4 specimens is 5.67, 6.02, 5.81, and 5.56 GPa, respectively.

Fig. 7 shows TEM microstructures of γ/α_2 lamellae in the Mo-TiAl alloys, and the interlamellar space can be measured by the line-cutting method. The measured interlamellar spacing of TNM1, TNM2, TNM3, and TNM4 specimens is 417±24, 338±16, 379±21, and 423±29 nm, respectively. It is found that adding the Mo element within 1.59at% can refine the interlamellar spacing. However, when the Mo addition is larger than 1.59at%, the γ/α_2 interlamellar spacing increases. Thus, the interlamellar spacing is negatively related to the nanoindentation hardness, i. e., the larger the interlamellar spacing, the smaller the nanoindentation hardness.

Wang et al[25] studied the nanoindentation hardness of the directionally solidified 4722 alloy, and found that the nanoindentation hardness (H_{nano}) and the interlamellar spacing have the power function relationship, as follows:

$$H_{nano} = a\lambda^b \quad (1)$$

where a and b are constants, and λ is the interlamellar spacing (nm). Substituting the nanoindentation hardness of TNM1, TNM2, TNM3, and TNM4 specimens and the measured interlamellar spacing into Eq.(1), the values of a and b can be

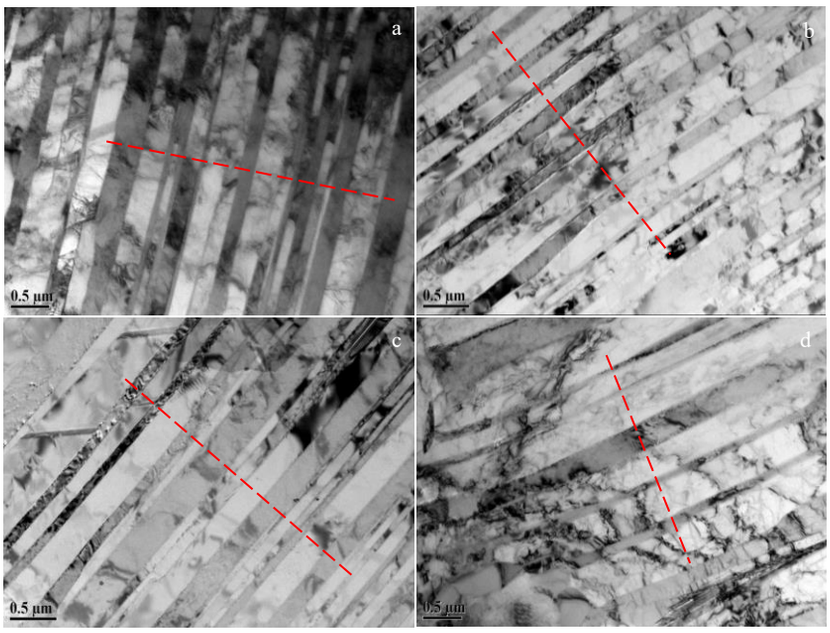

Fig.7 TEM microstructures of γ/α_2 lamellae in different Mo-TiAl alloys after HIP: (a) TNM1, (b) TNM2, (c) TNM3, and (d) TNM4

obtained by line fitting method as 40.01 and − 0.325 (R^2= 0.968), respectively. Thus, the relationship between nanoindentation hardness and interlamellar spacing can be expressed as follows:

$$H_{nano} = 40.01\lambda^{-0.325} \quad (2)$$

In the nanoindentation test, the indenter was pressed into the Mo-TiAl matrix, and the plastic deformation occurs near pressing position of the indenter. The main plastic deformation mechanism is the dislocation slip. When the interlamellar spacing is short, the dislocations encounter more γ/α_2 boundaries, increasing the hardness

2.4 Compression deformation behavior

Fig. 8 shows the flow stress-strain curves of different Mo-TiAl alloys after HIP during hot compression deformation at 1200 ℃ with a strain rate of 0.001 s^{-1}. The flow stresses of these four Mo-TiAl alloys all increase firstly and then slowly decrease. As the Mo content increases, the peak flow stress of the Mo-TiAl alloys gradually decreases. The change of the peak flow stress is related to the volume fraction variation of

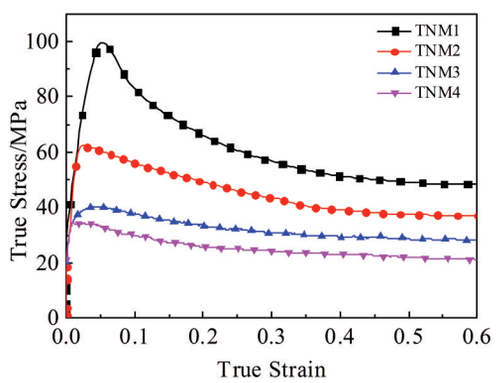

Fig.8 Flow stress-strain curves of different Mo-TiAl alloys after HIP

γ/α_2 lamellae. The average hardness of γ/α_2 lamellae is higher than that of the equiaxed γ and α_2 phases. The more the γ/α_2 lamellae in the alloy, the higher the strength and the more obvious the work hardening phenomenon. Correspondingly, the peak stress rises.

Table 4 shows the surface cracking states of the four Mo-TiAl alloys after hot compression deformation at 1200 ° C with different strain rates. It can be seen that the Mo-TiAl alloys have a tendency to crack during compression deformation at high strain rate (1 s^{-1}). As the strain rate decreases, the surface tends to be complete. For TNM3 and TNM4 specimens, when the strain rate increases to 0.01 and 0.001 s^{-1}, respectively, the surface cracks, indicating that their hot working deformation ability is inferior. According to Table 4, the hot workability of Mo-TiAl alloys is ranked from the best to the worst: TNM2>TNM1>TNM3>TNM4.

Fig. 9 shows the microstructures of different as-HIPed Mo-TiAl alloys after hot compression deformation. Under the hot compression deformation condition of 1200 ℃/0.01 s^{-1}, the lamellae in TNM1 and TNM2 specimens are transformed into the equiaxed α phase, which is relatively uniform. In TNM2 specimen, the residual β phase perpendicular to the hot

Table 4 Surface cracking of different Mo-TiAl alloys after HIP during hot compression deformation at 1200 ° C with different strain rates

Strain rate/s^{-1}	1	0.1	0.01	0.001
TNM1	×	√	√	√
TNM2	√	√	√	√
TNM3	×	×	×	√
TNM4	×	×	×	×

Note: × means that the specimen surface is cracked; √ means that the specimen surface is complete without obvious cracks

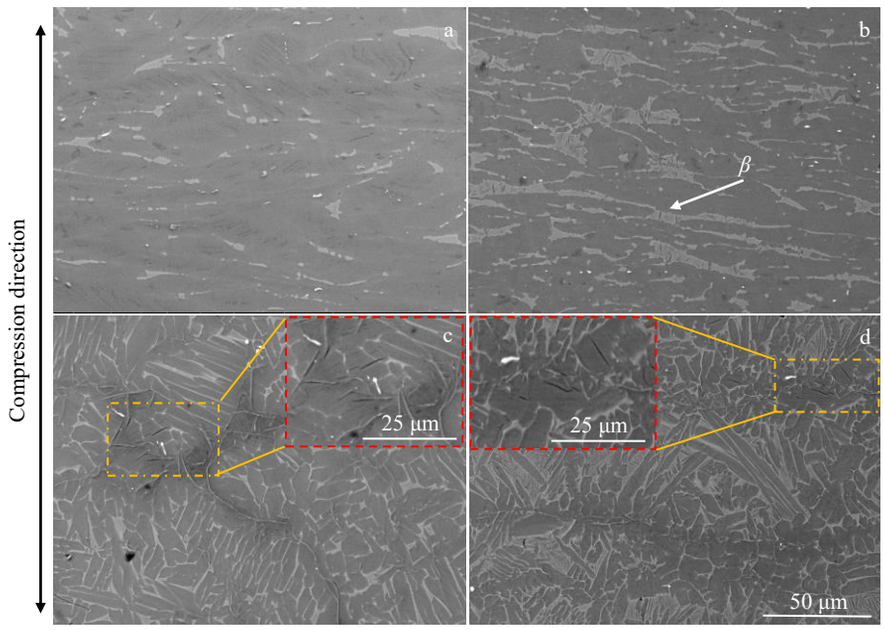

Fig.9 Microstructures of different as-HIPed Mo-TiAl alloys after hot compression deformation: (a) TNM1, (b) TNM2, (c) TNM3, and (d) TNM4

compression direction can also be observed (Fig. 9a and 9b). In TNM3 and TNM4 specimens, the microstructure is mainly composed of equiaxed γ and β phases, and the black mush zones appear after compression deformation. It can be seen that these mush zones consist of some residual γ/α_2 lamellae and equiaxed γ phase. Around these mush zones, a large number of microcracks appear, and the direction of crack initiation and propagation is consistent with the orientation of the γ/α_2 lamellae.

Fig. 10 shows the SEM microstructure and energy disperse spectroscope (EDS) line scanning results of the mush zone in TNM3 specimen. The mush zone is rich in Al, and has a small amount of Ti, Nb, and Mo (Fig. 10b), which is closely related to the S-type segregation in the Mo-TiAl alloys. The existence of microcracks near the mush area explains the sawtooth fluctuations in the flow stress of TNM3 and TNM4 specimens (Fig. 8)[26]. This phenomenon also corresponds to the inferior hot workability of TNM3 and TNM4 specimens. For TNM1 specimen, its hot workability is not as good as that of TNM2 specimen, mainly because TNM2 specimen contains more β phases. The β phase has a body-centered cubic structure, so the dislocations are easy to initiate, thus playing a coordinating role in the deformation process. Meanwhile, according to the hot compression performance of TNM3 and TNM4 specimens, the more β phases in alloy do not necessarily lead to the better plasticity of alloy. On the one hand, during high-temperature deformation, the β phase needs to be introduced, but it is also necessary to fully consider the uniformity of the microstructure and chemical composition to avoid composition segregation caused by the excessive addition of β phase stabilization elements. On the other hand, too much β phase will be transformed into the B2 phase at room temperature, resulting in inferior plasticity and creep properties at room temperature. If the β/B2 phase cannot be controlled by

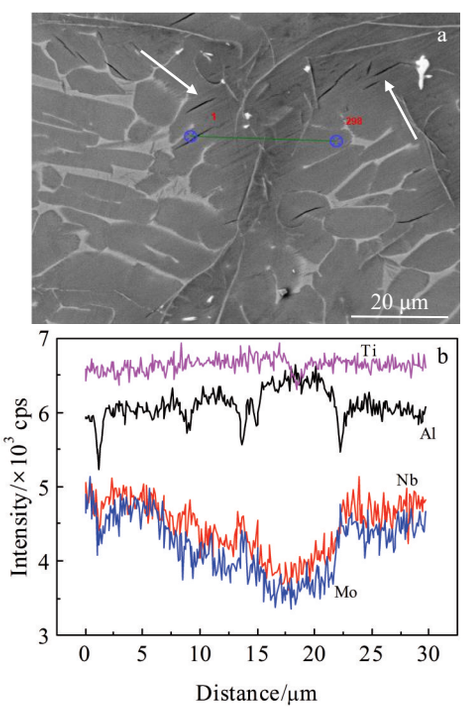

Fig.10 SEM microstructure (a) and EDS line scanning along marked greenline (b) in TNM3 specimen (for display convenience, the intensity of EDS spectra of Nb and Mo elements is increased by 5 times than the original intensity)

effective heat treatment, it is difficult for TiAl alloys to achieve ideal mechanical properties at room temperature.

3 Conclusions

1) The TiAl alloys containing Mo element of 1.02at% ,

1.59at% , 2.11at% , 3.94at% are named as TNM1, TNM2, TNM3, and TNM4 specimens, respectively, which are composed of γ, α_2, and β phases. As the content of Mo element increases, the content of the γ phase is gradually decreased, while that of the β phase is increased significantly. After the hot isostatic pressing (HIP) treatment, the γ phase around the lamellae increases, the TNM1 and TNM2 specimens have uniform microstructures, while the S-type segregation exists in the TNM3 and TNM4 specimens.

2) The atomic ratios of Ti/Al in the γ, α_2, and β phases are 0.96~1.04, 1.11~1.44, and 1.31~1.47, respectively. The added Mo element mainly exists in the β phase, and the content of Mo element in the β phase is increased with increasing the Mo addition. After HIP, the Mo content in the γ and α_2 phases is decreased slightly, and that in the β phase is increased, indicating that Mo element is diffused from the γ and α_2 phases to the β phase.

3) With the addition of Mo element, the nanoindentation hardness of the Mo-TiAl alloys is firstly increased and then decreased, reaching the maximum hardness with the Mo content of 1.59at%. The relationship between nanoindentation hardness and interlamellar spacing (λ) of Mo-TiAl alloys is $H_{\text{nano}} = 40.01\lambda^{-0.325}$.

4) The addition of the Mo element decreases the flow stress of Mo-TiAl alloys. During the hot compression at a high strain rate, the microcracks appear on the surface of TNM1, TNM3, and TNM4 specimens. The hot deformation ability of these four specimens from excellent to poor is arranged as follows: TNM2>TNM1>TNM3>TNM4. The poor hot workability of TNM3 and TNM4 specimens is due to the element segregation and uneven microstructure in alloys.

References

1 Li H, Yang C, Sun L X *et al. Materials Letters*[J], 2017, 187: 4
2 Sallot P, Monchoux J P, Joulié S *et al. Intermetallics*[J], 2020, 119: 106 729
3 Tian S W, Jiang H T, Guo W Q *et al. Intermetallics*[J], 2019, 112: 106 521
4 Li Haiyan, Kou Peipei, Li Longlong. *Rare Metal Materials and Engineering*[J], 2020, 49(5): 1593
5 Li Haiyan, Qiao Haiyang, Feng Ruicheng *et al. Rare Metal Materials and Engineering*[J], 2020, 49(6): 1931
6 Song L, Appel F, Wang L *et al. Acta Materialia*[J], 2020, 186: 575
7 Chlupová A, Heczko M, Obrtlík K *et al. Materials Science and Engineering A*[J], 2020, 786: 139 427
8 Gu X, Cao F Y, Liu N *et al. Journal of Alloys and Compounds* [J], 2020, 819: 153 264
9 Yadav M K, Siddiquee A N, Khan Z A. *Metals and Materials International*[J], 2021, 27(7): 2378
10 Jiang H T, Tian S W, Guo W Q *et al. Materials Science and Engineering A*[J], 2018, 719: 104
11 Imayev R M, Imayev V M, Oehring M *et al. Intermetallics*[J], 2007, 15(4): 451
12 Banumathy S, Neelam N S, Chandravanshi V *et al. Materials Today: Proceedings*[J], 2018, 5(2): 5514
13 Han J C, Xiao S L, Tian J *et al. Materials Characterization*[J], 2015, 106: 112
14 Han J C, Liu Z D, Jia Y *et al. Vacuum*[J], 2020, 174: 109 210
15 Chen Y Y, Li B H, Kong F T. *Journal of Alloys and Compounds* [J], 2008, 457(1-2): 265
16 Xu W C, Zhang H, Shan D B. *Journal of Zhejiang University-Science A*[J], 2010, 11(10): 738
17 Clemens H, Mayer S. *Advanced Engineering Materials*[J], 2013, 15(4): 191
18 Cha L, Clemens H, Dehm G. *International Journal of Materials Research*[J], 2011, 102(6): 703
19 Chen G L, Xu X J, Teng Z K *et al. Intermetallics*[J], 2007, 15(5-6): 625
20 Liu G H, Wang Z D, Fu T L *et al. Journal of Alloys and Compounds*[J], 2015, 650: 45
21 Dong S L, Liu T, Li Y J *et al. Vacuum*[J], 2019, 159: 391
22 Jiang C. *Acta Materialia*[J], 2008, 56(20): 6224
23 Huang Zunixng, Wang Xiuli, Zhou Lixin *et al. Chinese Journal of Structural Chemistry*[J], 2002, 21(2): 218 (in Chinese)
24 Holec D, Reddy R K, Klein T *et al. Journal of Applied Physics* [J], 2016, 119(20): 205 104
25 Wang Qiang. *Thesis for Doctorate*[D]. Harbin: Harbin Institute of Technology[D], 2018 (in Chinese)
26 Cao Hui, Rui Zhiyuan, Chen Wenke *et al. Molecular Simulation* [J], 2018, 44(18): 1489

Mo元素含量对TiAl合金微观组织及力学性能的影响

田世伟[1]，何安瑞[1]，刘建华[1]，张业飞[1]，张　韵[1]，杨永刚[1,2]，王家毅[3]，江海涛[1]

(1. 北京科技大学 工程技术研究院，北京 100086)

(2. 瑞典皇家理工学院 材料科学与工程学院，瑞典 斯德哥尔摩 SE-10044)

(3. 烟台南山学院 工学院，山东 烟台 265713)

摘　要：设计了4种不同Mo含量的TiAl合金，使用扫描电子显微镜、纳米压痕、热模拟压缩等手段对Mo-TiAl合金的微观组织以及力学性能进行了研究。结果显示，随着Mo含量升高，组织中γ相含量逐渐减少，而β相含量逐渐增多。Mo元素主要以β相的形式存在于TiAl合金中。在热等静压过程中，Mo元素从γ相和α_2相向β相中扩散；Mo-TiAl合金的纳米压痕硬度在Mo含量为1.59%（原子分数，下同）时达到最大，并且纳米压痕硬度和片层间距呈负相关；随着Mo含量升高，Mo-TiAl合金热压缩流变应力降低，Mo含量为2.11%和3.94%的TiAl合金由于Al元素偏析导致其塑性较差。

关键词：TiAl合金；Mo元素；微观组织；纳米压痕；偏析

作者简介：田世伟，男，1993年生，博士，北京科技大学工程技术研究院，北京 100083，电话：010-62332598-6828，E-mail：b2067810@ustb.edu.cn